JACS
JOURNAL OF THE AMERICAN CHEMICAL SOCIETY
Article
pubs.acs.org/JACS

A Slowly Relaxing Rigid Biradical for Efficient Dynamic Nuclear Polarization Surface-Enhanced NMR Spectroscopy: Expeditious Characterization of Functional Group Manipulation in Hybrid Materials

Alexandre Zagdoun,[†] Gilles Casano,[‡] Olivier Ouari,[‡] Giuseppe Lapadula,[§] Aaron J. Rossini,[†] Moreno Lelli,[†] Mathieu Baffert,[∥] David Gajan,[§] Laurent Veyre,[∥] Werner E. Maas,[⊥] Melanie Rosay,[⊥] Ralph T. Weber,[⊥] Chloé Thieuleux,[∥] Christophe Copéret,[§] Anne Lesage,[†] Paul Tordo,*[,‡] and Lyndon Emsley*[,†]

[†]Centre de RMN à Très Hauts Champs, Université de Lyon (CNRS/ENS Lyon/UCB Lyon 1), 69100 Villeurbanne, France
[‡]SREP LCP UMR 6264, Aix Marseille Universities, Faculté de Saint Jérôme, 13013 Marseille, France
[§]Department of Chemistry, Laboratory of Inorganic Chemistry, ETH Zürich, CH-8093, Zürich, Switzerland
[∥]Institut de Chimie de Lyon, C2P2, CNRS/UCB Lyon 1/ESCPE Lyon, 69100 Villeurbanne, France
[⊥]Bruker BioSpin Corporation, Billerica, Massachusetts 01821, United States

Supporting Information

ABSTRACT: A new nitroxide-based biradical having a long electron spin−lattice relaxation time (T_{1e}) has been developed as an exogenous polarization source for DNP solid-state NMR experiments. The performance of this new biradical is demonstrated on hybrid silica-based mesostructured materials impregnated with 1,1,2,2-tetrachloroethane radical containing solutions, as well as in frozen bulk solutions, yielding DNP enhancement factors (ε) of over 100 at a magnetic field of 9.4 T and sample temperatures of ∼100 K. The effects of radical concentration on the DNP enhancement factors and on the overall sensitivity enhancements ($\Sigma^{\dagger}$) are reported. The relatively high DNP efficiency of the biradical is attributed to an increased T_{1e}, which enables more effective saturation of the electron resonance. This new biradical is shown to outperform the polarizing agents used so far in DNP surface-enhanced NMR spectroscopy of materials, yielding a 113-fold increase in overall sensitivity for silicon-29 CPMAS spectra as compared to conventional NMR experiments at room temperature. This results in a reduction in experimental times by a factor >12 700, making the acquisition of ^{13}C and ^{15}N one- and two-dimensional NMR spectra at natural isotopic abundance rapid (hours). It has been used here to monitor a series of chemical reactions carried out on the surface functionalities of a hybrid organic−silica material.

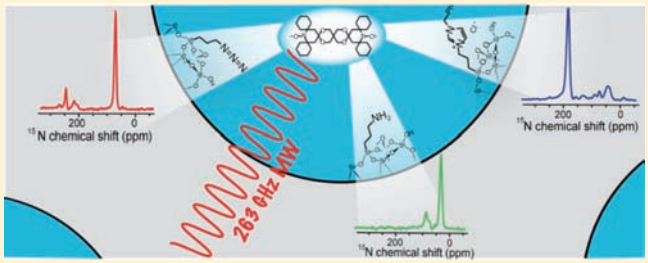

INTRODUCTION

Nuclear magnetic resonance (NMR) is one of the richest sources of structural and dynamic information for molecular and materials sciences. However, it is traditionally limited by its intrinsic poor sensitivity. Dynamic nuclear polarization (DNP) has in principle the potential to increase NMR sensitivity by orders of magnitude by transferring polarization from unpaired electrons to nuclei. First discovered in the 1950s with low magnetic fields,[1−3] high-field DNP NMR experiments are now possible with gyrotron sources, which are capable of delivering high-power high-frequency microwaves (MW).[4,5] In this respect, in the past few years, DNP-enhanced solid-state NMR spectroscopy under magic angle spinning (MAS) conditions has made great progress, and DNP signal enhancement factors (ε) of up to ∼250 have been reported at high fields (up to 9.4 T) and low temperatures (<100 K) for biological solids[6−13] as well as for hybrid or inorganic materials.[14−17] The dramatic sensitivity gain provided by the DNP approach has thus enabled the determination of the interstrand architecture of amyloid fibrils[11−13] and the elucidation of the bonding topologies at the surface of functionalized mesostructured materials.[15] In this approach, samples are dissolved or impregnated with a solution containing stable exogenous paramagnetic centers such as nitroxides or trityls,[18] which act as polarizing agents. Most high-field solid-state DNP NMR experiments are carried out in the presence of biradical polarizing agents[19] as they can transfer polarization through the cross-effect (CE) mechanism, which is

Received: October 25, 2011
Published: December 19, 2011

 © 2011 American Chemical Society dx.doi.org/10.1021/ja210177v | J. Am. Chem.Soc. 2012, 134, 2284−2291

currently the most efficient mechanism for DNP at high fields.[20]

The CE relies upon having a three-spin system consisting of two dipolar coupled electrons and a nucleus. For polarization transfer to occur from the electrons to the nucleus upon saturation of one of the EPR frequencies, the two unpaired electrons should have a significant dipolar coupling, and their EPR frequencies must differ by the nuclear Larmor frequency (here proton).[18]

Initial CE high-field DNP experiments were performed with solutions doped with high concentrations of monoradical species, such as TEMPO.[21] Much effort has been recently devoted to the design and synthesis of more efficient radicals for DNP.[21−24] Griffin and co-workers demonstrated that biradical polarizing agents yielded significant improvements in the DNP process, and therefore in the sensitivity enhancement factors.[19] The success of biradicals is primarily attributed to the uniformly short distance between the two unpaired electrons in a biradical, which guarantees that all unpaired electrons are dipolar coupled to at least one other electron. With nitroxide-based biradicals, the EPR frequency difference is provided by *g*-anisotropy, and the difference in EPR frequencies can match the ^{1}H Larmor frequency when the g_{xx} (or g_{yy}) component of the **g** tensor of one of the unpaired electrons is parallel to the g_{yy} (g_{zz}) component of the other.[25,26] Recently, triradical,[23] heterogeneous biradical species or mixtures of radical species,[27,28] and metal ions[29] have been proposed as alternatives to dinitroxide polarizing agents.

The water-soluble biradical TOTAPOL[22] (Figure 1d) is today the most commonly employed exogenous polarizing agent in DNP solid-state NMR, in particular for biological applications.[30] TOTAPOL was shown, however, to have a relatively flexible structure,[25] and as a result the frequency matching condition for the CE mechanism is only properly fulfilled for the fraction of the biradicals that adopts the correct conformation. Another step forward was achieved by Griffin, Tordo, and co-workers who introduced bTbK[26] (Figure 1e), a binitroxide radical in which the two TEMPO molecules are linked by a rigid tether. The rigid tether constrains the orientation of the TEMPO moieties, such that the g_{zz} components of the two **g**-tensors are roughly orthogonal. It was demonstrated that bTbK provides DNP enhancement factors, which are 1.4 times larger than TOTAPOL under similar conditions.[26] We have more recently shown that this biradical may be readily combined with organic solvents for the investigation of water incompatible materials.[31]

The electron spin−lattice relaxation time T_{1e} is another factor that impacts the DNP process. It is known that a longer T_{1e} facilitates saturation of the EPR transition.[21,32] This effect partially accounts for the improved DNP at lower sample temperature,[5,33] because electron relaxation rates slow significantly with temperature.[34,35] However, this factor has not been so far considered directly in the design of biradicals for DNP.

In this Article, we introduce a new biradical, bis-cyclohexyl-TEMPO-bisketal (bCTbK, Figure 1f), a bulky derivative of bTbK, in which the geminal dimethyl groups have been replaced by spirocyclohexyl moieties. In agreement with previous relaxation rate measurements on spirocyclohexyl functionalized nitroxide radicals,[35] we show that, in 1,1,2,2-tetrachloroethane ("tetrachloroethane") at 100 K, bCTbK has a T_{1e} value that is almost twice as long as that for bTbK. On a model hybrid mesostructured silica-based material,[14,36] we

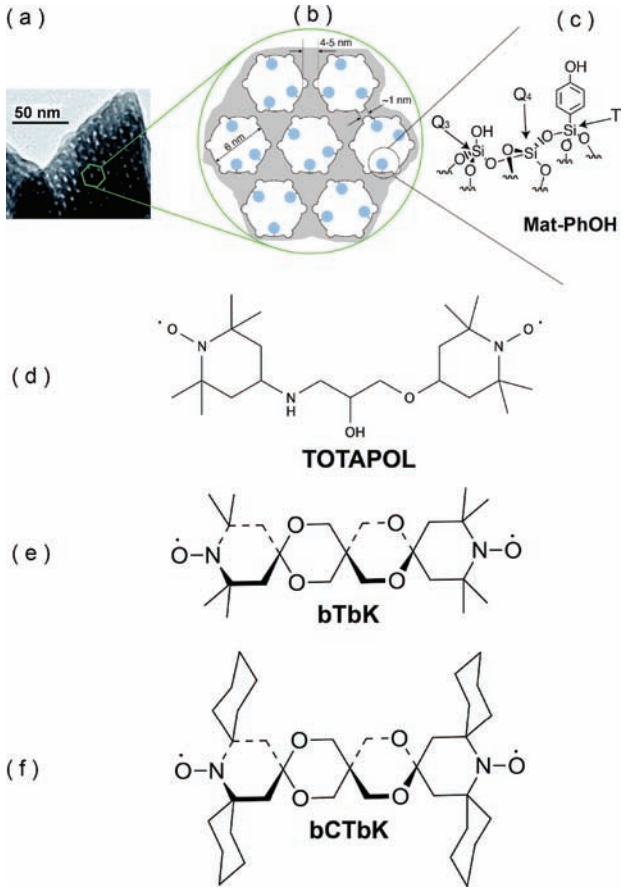

Figure 1. (a) Transmission electron microscopy image of the hybrid mesostructured silica material studied here. (b) Schematic representation of the pores. The blue circle represents the organic moieties present on the mesoporous surface. The shaded gray area represents the bulk silica. (c) Structure of **Mat-PhOH**.[36] Different types of silicon atoms present at the surface are labeled here. (d−f) Structures of TOTAPOL, bTbK, and bCTbK.

show that this biradical yields proton and silicon-29 cross-polarization (CP) DNP enhancement factors that are between 2.5 and 4 times larger than bTbK. The reduction in experimental times provided by DNP experiments with bCTbK further pushes back the limits of solid-state NMR spectroscopy in terms of sensitivity, notably for the structural investigation of dilute surface species. This polarizing mixture is directly applicable to study a wide range of problems. We show here that with the high sensitivity provided by DNP with bCTbK, it becomes possible to expediently monitor the stepwise functionalization at the surface of hybrid materials by ^{1}H, ^{13}C, ^{29}Si, as well as ^{15}N solid-state NMR spectroscopy at natural isotopic abundance. Notably, high-quality one-dimensional ^{15}N solid-state NMR spectra can be acquired with experiment times on the order of 1 h, and two-dimensional ^{1}H−^{15}N HETCOR spectra can be acquired in less than 12 h.

■ EXPERIMENTAL SECTION

Synthesis and characterization of the hybrid mesostructured silica materials are described in the Supporting Information. The biradical TOTAPOL was purchased in crystalline form from DyNuPol Inc., MA, and used without further purification. The solvents were purchased from Sigma-Aldrich and used without further purification.

Synthesis of bCTbK. bCTbK was prepared in a four-step sequence starting from 2,2,6,6-tetramethylpiperidin-4-one. The 2,6-

dx.doi.org/10.1021/ja210177v | J. Am. Chem.Soc. 2012, 134, 2284−2291

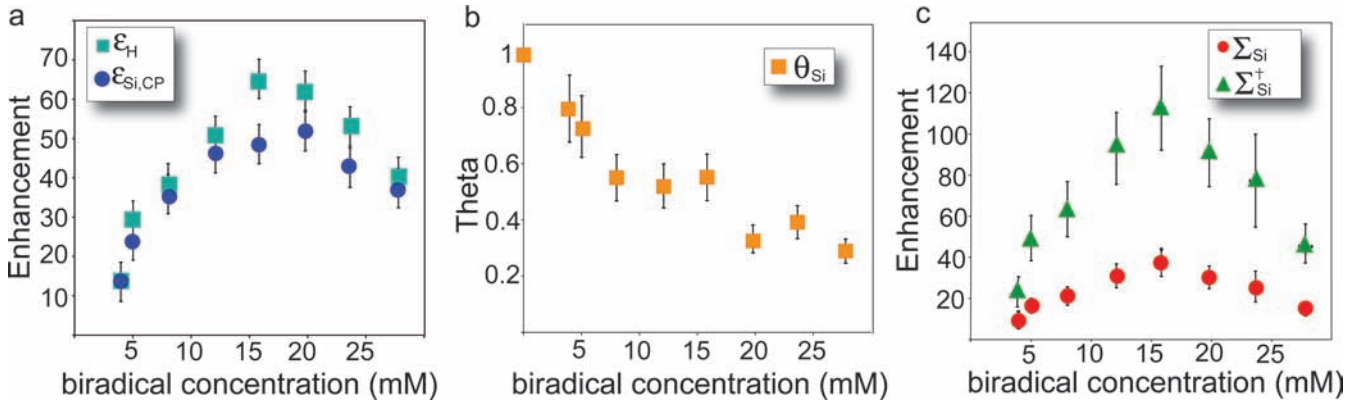

Figure 2. (a) Proton DNP (ε_H) and silicon DNP enhancement ($\varepsilon_{Si,CP}$). (b) The ^{29}Si quenching factor (θ_{Si}) shown as a function of bCTbK concentration in 1,1,2,2-tetrachloroethane. (c) Overall ($\Sigma_{Si,CP}$ and $\Sigma^{+}_{Si,CP}$) sensitivity enhancements. Note that ε_H quantifies the enhancement of the solvent and $\varepsilon_{Si,CP}$ quantifies that of the surface. Experimental details and definition of the enhancement factors are given in the Supporting Information.

Table 1. DNP Efficiency Comparison and Electron Spin−Lattice Relaxation Times for the TOTAPOL, bTbK, and bCTbK Biradicals under Optimal Conditions

biradical	solvent	ε_H [a,b]	$\varepsilon_{Si,CP}$ [a,c]	$\Sigma_{Si,CP}$ [a,c]	$II_m(^{13}C)$ [b,d]	T_{1e} [e] (μs)	T_{2e} [e] (μs)
TOTAPOL	water	– [f]	31(3)	15(4)	0.75(3)	554(4)	1.6(1)
bTbK	tetrachloroethane	26(3)	21(3)	12(5)	0.51(2)	453(4)	1.5(1)
bCTbK	tetrachloroethane	105(3)	52(3)	38 (7)	1.00(4)	762(4)	2.8(1)

[a]Measured on **Mat-PhOH** impregnated with a 16 mM biradical solution. Estimated errors are given in parentheses. [b]Recorded on a triple resonance CPMAS probe at 99 K. The difference of DNP efficiency between the two probes can be attributed to differences of the hardware (e.g., waveguide efficiency and alignment) and the lower temperature that could be reached with the triple resonance probe. See the Supporting Information for a more detailed characterization of the DNP efficiency dependence on the biradical concentration on this probe. This explains the discrepancy between ε_H and ε_{Si} for bCTbK in tetrachloroethane. [c]Recorded on a double resonance CPMAS probe at 102 K. [d]In this case, it is not possible to quantify the overall sensitivity enhancement for carbon due to the fact that it is impossible to obtain a MW off carbon spectrum with high enough S/N ratio to calculate reliable integrals in a reasonable experimental time. However, it is possible to compare the relative efficiency of the different biradicals for enhancing the carbon resonances by comparing the integrated intensities per unit of mass (II_m). Here, the II_m values of the aromatic resonances of **Mat-PhOH** impregnated with the various biradical containing solutions are displayed. The concentration of the bTbK and TOTAPOL solutions was 12 mM, and the bCTbK one was a 16 mM solution (concentration giving optimal sensitivity for each biradical). The II_m of **Mat-PhOH** impregnated with a 16 mM solution of bCTbK in tetrachloroethane was taken as a reference. [e]Electron spin−lattice (T_{1e}) and spin−spin (T_{2e}) relaxation times were measured on the edge of the EPR line in a frozen bulk solution at 90 K with 8 mM biradical concentration at an EPR resonance frequency of 94 GHz. For TOTAPOL, glycerol was added to water to form a glass (60%/40% glycerol/H_2O by volume). [f]The ^{1}H resonance of water is too broad to calculate a reliable proton DNP enhancement.

cyclohexyl-substituted piperidin-4-one **2** (see the Supporting Information) was prepared according to the method described by Yamada and Utsumi[37] and was then reacted with pentaerythritol to afford the spirodiamino precursor of bCTbK. Subsequent oxidation of the spirodiamino precursor by hydrogen peroxide in the presence of sodium tungstate provided the dinitroxide bCTbK (see the Supporting Information for further experimental details).

Sample Preparation for NMR Experiments. Samples were prepared by impregnating 8.9−9.8 mg of dry powder with ca. 17 μL of a radical containing solution. The total mass of impregnated material was determined, and the sample was mixed using a glass-stirring rod to obtain a homogeneous distribution of the radical containing solution in the powder. The impregnated powder was then packed into a 3.2 mm sapphire NMR rotor to maximize MW penetration into the sample. The mass of impregnated material inside the rotor was determined, and a tight polyfluoroethylene plug was inserted to prevent any leakage of the solvent during spinning. The rotor was capped with a zirconia drive tip and quickly inserted into the DNP spectrometer. See http://pubs.acs.org/JACSbeta/scivee/index.html#video2 for a video demonstration of the sample preparation procedure.

Solid-State NMR Spectroscopy. All spectra were acquired on a Bruker Avance III 400 MHz DNP NMR spectrometer equipped with a 263 GHz gyrotron microwave system[5] (B_0 = 9.4 T, $\omega_H/2\pi$ = 400 MHz, $\omega_C/2\pi$ = 100 MHz, $\omega_{Si}/2\pi$ = 79.5 MHz). The field sweep coil of the NMR magnet was set so that MW irradiation occurred at the DNP enhancement maximum of TOTAPOL (263.334 GHz), with an estimated 4 W power of the MW beam at the output of the probe waveguide. ^{29}Si spectra and ^{1}H spectra of **Mat-PhOH** impregnated with radical containing solutions were recorded using a double resonance low-temperature CPMAS probe with a sample spinning frequency of 8 kHz and a sample temperature of 102 K. ^{1}H, ^{13}C, and ^{15}N spectra were recorded using a triple resonance low-temperature CPMAS probe with a sample temperature of 99 K and sample spinning frequencies of 12 kHz for the ^{13}C spectra and 8 kHz for the ^{15}N spectra. SPINAL-64[38] heteronuclear decoupling was applied during acquisition ($\omega_{1H}/2\pi$ = 89 kHz). Additional experimental details are provided in the Supporting Information. Pulse programs are available on request. Processing of the spectra was done using the Topspin software package, and fitting of NMR relaxation measurements was done using Kaleidagraph.

EPR Spectroscopy. All measurements were conducted at W band (94 GHz EPR frequency) on a Bruker Elexsys E680 EPR spectrometer, with sample temperatures of 90 K. T_{1e} was measured using inversion−recovery sequences, and the curves were fitted with biexponential functions to obtain T_{1e}. The slow component of the fit is identified as T_{1e}, while the fast component (<90 μs) is attributed to spectral diffusion and is not reported here.

RESULTS AND DISCUSSION

bCTbK DNP Efficiency. The DNP efficiency of bCTbK was evaluated by impregnating a model mesoporous silica-based material **Mat-PhOH**[36] containing phenolic ligands incorporated at the surface of the pores ((Figure 1a–c). The material was impregnated with bCTbK containing tetrachloroethane solutions of various concentrations. Tetracholorethane was used because we have previously shown that this solvent provides optimal DNP enhancements (ε) for bTbK.[31] Figure 2a displays the dependence of the proton (ε_H) and silicon ($\varepsilon_{Si,CP}$) DNP enhancement on the radical concentration (where ε is defined as the ratio of the integrated intensities of the spectra acquired with and without microwave irradiation under otherwise identical conditions). ε_H is found to peak at 65 for a radical concentration of 15.8 mM (similar to optimum concentrations previously observed for other biradicals).[17,31] $\varepsilon_{Si,CP}$ peaks at 52 for a concentration of 19.8 mM. The difference between the silicon enhancement at 15.8 and 19.8 mM is small, so the offset between the optimal concentration for proton and silicon is within experimental error. Note these curves were obtained with a double-resonance probe at 102 K. Higher enhancements for proton were obtained with a triple resonance probe at 99 K (see Table 1, footnote b, Figure 3, and Figure S2), with ε_H peaking at 105 for **Mat-PhOH** impregnated with a 16 mM bCTbK solution in tetrachloroethane (note that an enhancement of 105 corresponds to a 1% proton polarization at 400 MHz and 99 K, as compared to 0.0097% for the thermal equilibrium polarization, without DNP). The increased ε observed with a different probe was attributed to the slightly lower sample temperatures as well as to slightly higher MW power at the sample.

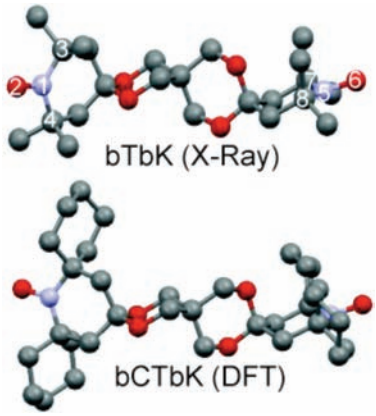

Figure 3. Comparison between the X-ray structure of bTbK and the DFT optimized geometry of bCTbK (optimized at the B3LYP/6-31G(d,p) level).

Note that ε quantifies the observed DNP efficiency, but it does not take into account factors such as the reduction in NMR signal intensity or changes in longitudinal relaxation times caused by the introduction of a paramagnetic radical in the sample.[17,23] We have recently shown how the equivalent fraction of NMR active nuclei that contributes to the NMR signal (the quenching factor θ) can be experimentally measured, and we introduced overall sensitivity enhancement factors Σ and $\Sigma^{\dagger}$, which take into account these parameters.[17] The factor $\Sigma^{\dagger}$ also takes into account the additional sensitivity enhancement (Boltzmann) factor of ~3 obtained by carrying out the experiments at 100 K rather than at room temperature (the calculation of these factors here is detailed in Table S3).[17] $\Sigma^{\dagger}$ is an estimation of the overall gain in sensitivity obtained by carrying out low-temperature DNP solid-state NMR experiments instead of conventional room-temperature experiments.[17]

As expected, and as previously observed on other systems, θ diminishes as the radical concentration increases (Figure 2b).[17,31] Here, however, quenching appears to be less than for water/TOTAPOL with θ = 0.39 for **Mat-PhOH** impregnated with a 12 mM solution of TOTAPOL in water and 0.54 for a 12 mM solution of bCTbK in tetrachloroethane. Figure 2c displays the overall sensitivity enhancements for silicon with ($\Sigma^{\dagger}_{Si,CP}$) and without ($\Sigma_{Si,CP}$) the Boltzmann factor as a function of the radical concentration.

$\Sigma_{Si,CP}$ and $\Sigma^{\dagger}_{Si.CP}$ peak at 15.8 mM with a value of 38 and 113, respectively. As expected, $\Sigma_{Si,CP}$ is always lower than $\varepsilon_{Si,CP}$ as it accounts for the decrease in θ and $T_1(^1H)$ with increasing radical concentration (Figure S3), the latter meaning that more scans can be acquired in the same amount of time. A value of $\Sigma^{\dagger}$ = 113 translates into a reduction in experimental time by a factor of 12 700 as compared to ordinary room-temperature experiments.

Performance in Frozen Bulk Solutions and Other Solvents. bCTbK also provides high enhancements in frozen bulk solution (ε_H = 63, $\varepsilon_{C,CP)}$ = 67, Figure S4), as compared to ε_H = 22 for bTbK.[31]The high enhancements provided by bCTbK also mean that reasonable ε of ~30 can be obtained for nonoptimal solvents (e.g., ε_H = 23 and $\varepsilon_{Si,CP}$ = 26 for a 12 mM solution of bCTbK in mesitylene as opposed to ε_H = 6 for a 10 mM solution of bTbK in mesitylene,[31] both impregnated in **Mat-PhOH**, Figure S5). This therefore extends the number of solvents that can be used for DNP experiments, which is a necessity if chemically reactive systems are to be studied by DNP SENS in the future.

Comparison with Previously Used Biradicals. Under the same experimental conditions, both TOTAPOL and bTbK are found to be typically less efficient than bCTbK ($\varepsilon_{Si,CP}$ = 31 for TOTAPOL/water and $\varepsilon_{Si,CP}$ = 21 for bTbK/tetrachloroethane, both impregnated within **Mat-PhOH**, Table 1). With $\varepsilon_{Si,CP}$ = 52, **Mat-PhOH** impregnated with bCTbK solutions provides the best enhancement obtained so far under any conditions for this model material. This corresponds to an improvement in the DNP efficiency by a factor of about 2.5 with respect to bTbK in tetrachloroethane.

We attribute the improved performance of the bCTbK biradical mainly to more favorable electron relaxation times. The DNP efficiency of biradicals has been shown to be significantly dependent on T_{1e}, as a longer T_{1e} allows for a better saturation of the EPR line, therefore increasing the DNP effect.[21,23,32] The effect of higher electron saturation on the DNP enhancement has previously been demonstrated by Thurber et al. by using field-modulation during the polarization buildup.[23] To the best of our knowledge, biradicals have not been previously developed for use as DNP polarizing agents to specifically have long relaxation times. We designed the bCTbK biradical to benefit from the optimal geometry of bTbK, while also having longer relaxation times. The methyl groups around each nitroxide center in bTbK were replaced with spirocyclohexyl groups in bCTbK, increasing the size and rigidity of the radical. Both the low-temperature and the room-temperature EPR spectra of bTbK and bCTbK dissolved in tetrachloroethane are similar, which suggests that the **g** and **A** tensors of both biradicals are similar.

Because bCTbK has not yet yielded crystals suitable for diffraction, to confirm that the structures of these two spiro radicals are similar, the geometry of both radicals was optimized with DFT calculations (Figure 3, Table 2). The accuracy of the

Table 2. Distances, Angle, and Dipolar Coupling for bTbK and bCTbK

compound	d_{N-O} (Å)[a]	d_{O-O} (Å)[b]	d_{N-N} (Å)[c]	ψ[d]	D[e] (MHz)
bTbK (X-ray)	1.283	13.030	10.777	79.57	30.9
	1.289				
bTbK (DFT[f])	1.285	13.342	11.034	80.36	28.8
	1.286				
bCTbK (DFT[f])	1.285	13.249	10.990	77.56	29.3
	1.286				

[a]N−O bond length of the two nitroxides. [b]O_1-O_5 distance. [c]N_2-N_6 distance. [d]Angle between the mean $C_3N_1O_2C_4$ and $C_7N_5O_6C_8$ planes. [e]From the dipole point approximation (D = 52 160/d_{ee}, where d_{ee} is the mean electron−electron distance). [f]Optimized at the B3LYP/6-31G(d,p) level.

calculations was confirmed by noting that the calculated geometry of bTbK closely matches that obtained from its single-crystal X-ray diffraction structure (Table 2). DFT calculations show that bTbK and bCTbK share analogous structures: (i) the calculated angles ψ between the mean planes $C_3N_1O_2C_4$ and $C_7N_5O_6C_8$ (Figure 3) differ by less than 3°, and (ii) the intramolecular nitrogen−nitrogen (N_1-N_7) distances in bTbK and bCTbK are predicted to differ by only 0.044 Å. This suggests that the electron−electron dipolar couplings are on the order of 29 MHz and are nearly identical for both radicals.

Having confirmed that the major structural features and EPR tensor parameters for both bTbK and bCTbK are essentially the same, it is then clear that the improved DNP enhancements obtained with bCTbK can be mainly attributed to its slower electron relaxation. T_{1e} is found to be 1.7 times higher for bCTbK (762 μs) than for bTbK (453 μs) (Table 1) under otherwise identical conditions. It is known that for radicals in glassy organic solvents around 100 K, Raman processes are the dominant relaxation mechanism, suggesting that T_{1e} is likely to increase as the rigid size/molecular mass of the radical is increased.[34] It has also been observed that methyl groups lead to shorter transverse relaxation times.[35] We also note that the T_{1e} of bCTbK in tetrachloroethane is longer than that of TOTAPOL in water (554 μs), despite the fact that electron relaxation times of nitroxides in frozen solutions are known to increase with the polarity of the solvent.[34] A water-soluble version of bCTbK is expected to have an even longer T_{1e}, possibly leading to higher enhancements. The high DNP efficiency of bCTbK can thus be partially attributed to both its favorable orientation of the TEMPO moieties and its long T_{1e}. Note that T_{1e} is known to be anisotropic along the EPR line, and it has been measured in this study at the high-field edge of the spectrum, corresponding to the zone irradiated during DNP experiments.

Improved DNP efficiency may also arise from longer spin−spin relaxation times (T_{2e}), as T_{2e} has also been hypothesized to help maintain the frequency match condition for the CE.[21]

In summary, these results show the influence of electron relaxation times on the efficiency of polarizing agents and thus add another parameter to consider for further rational design of polarization agents for DNP experiments.

Monitoring Chemical Reactions on a Surface. Developing functional materials has become a major field of research in recent years due to their application in various areas such as catalysis, drug delivery, or gas purification. Understanding the structures and the chemical transformation of their surface functionalities at a molecular level is essential to provide reliable structure−property relationships, which are essential to the design and the controlled synthesis of the targeted functional materials. In this respect, solid-state NMR would be a method of choice, as it allows one to access structures, conformations, and dynamics of molecules, including surface species. However, the applicability of NMR is typically limited by its inherent low sensitivity, with the low concentration of the surface functionalities (typically <10 mmol/g), and the low natural abundance of most of the relevant NMR active nuclei (1% for carbon-13 and 0.3% for nitrogen-15).[39]

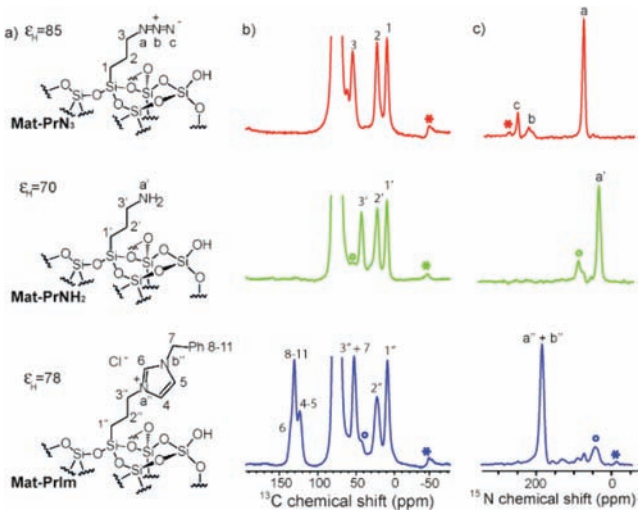

Figure 4. (a) Structure, (b) $^1H-^{13}C$ CP spectra, and (c) $^1H-^{15}N$ spectra of compounds **Mat-PrN3**, **Mat-PrNH2**, and **Mat-PrIm**. The most probable assignments based on the observed chemical shift resulting from this spectrum are shown. The asterisks indicate spinning sidebands, and the open circles note the presence of byproducts or incomplete conversion from the previous synthetic steps. The proton enhancements with a sample spinning frequency of 12 kHz are also reported. Experimental details are described in the text and in the Supporting Information.

We recently demonstrated that DNP SENS makes it possible to probe in acceptable experimental times (hours) the surfaces of various materials such as pure as oxides (silica,[16] alumina[40]), functionalized hybrid organic−inorganic silica materials,[14] functionalized silica nanoparticles,[15] and metal organic frameworks (MOFs)[41] at natural isotopic abundance. However, DNP enhancement factors rarely exceeded 40 in our hands. To demonstrate the potential of the large enhancements provided by the bCTbK polarizing mixture, we investigate the stepwise chemical transformation and the formation of imidazolium-containing materials (**Mat-PrIm**), which can be used as permanently immobilized "ionic liquids"[42−46] or as precursors to *N*-heterocyclic carbenes,[47,48] an important class of ligands for stable single-site catalysts (Figure 4a).

Here, the imidazolium unit was introduced by a stepwise postfunctionalization of **Mat-PrN$_3$** prepared by a direct

dx.doi.org/10.1021/ja210177v | J. Am. Chem.Soc. 2012, 134, 2284−2291

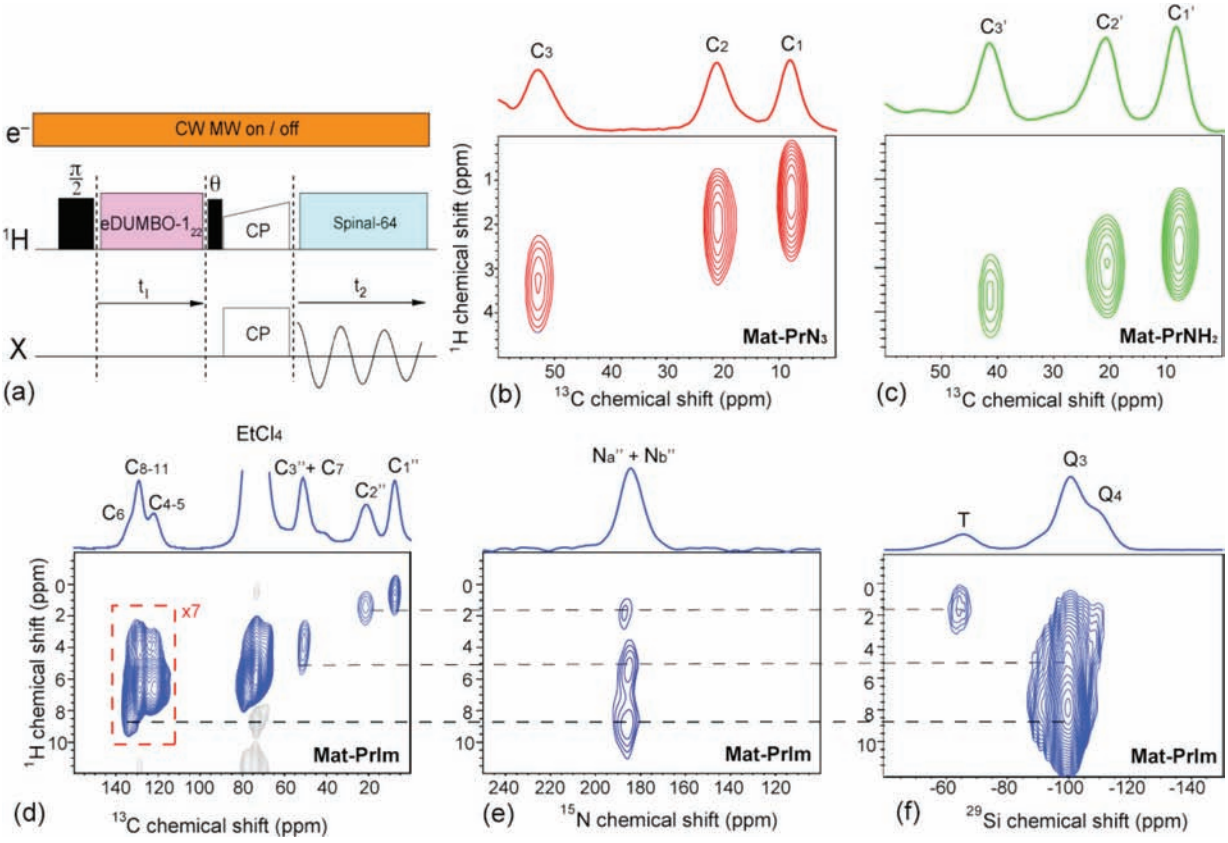

Figure 5. (a) Pulse sequence for the 2D SENS ^{1}H-X HETCOR experiments. (b–d) Contour plots of a 2D SENS ^{1}H–^{13}C HETCOR spectra of compounds **Mat-PrN$_3$**, **Mat-PrNH$_2$**, and **Mat-PrIm**, respectively. (e) Contour plot of a 2D DNP SENS ^{1}H–^{15}N HETCOR of **Mat-PrIm**. (f) Contour plot of a 2D DNP SENS ^{1}H–^{29}Si HETCOR of **Mat-PrIm**. All compounds were impregnated with a 16 mM solution of bCTbK in tetrachloroethane. The contact time was 100 μs for the ^{1}H–^{13}C experiments, 1 ms for the ^{1}H–^{15}N correlation experiments, and 250 μs for the ^{1}H–^{29}Si. During t_1, eDUMBO-1$_{22}$[51] homonuclear decoupling was applied.

synthesis approach.[49] This included a Staudinger reduction providing an aminopropyl unit in **Mat-PrNH$_2$** followed by its conversion into **Mat-PrIm** via reaction with formaldehyde, glyoxal, and benzylamine (Figure 4, see the Supporting Informatino for additional experimental details). Note that **Mat-PrN$_3$** was prepared by a direct synthesis approach, that is, by a cohydrolysis co-condensation of $(EtO)_3SiPrN_3$ and $(EtO)_4Si$ in the presence of a structure-directing agent, here Pluronic-P123. This allows the formation of high-surface area mesostructured materials as evidenced by TEM and N_2 adsorption experiments (see the Supporting Information) as well as the controlled site distribution of surface functionalities. Moreover, the nonpolar nature of azido group enables one to access a broad range of concentrations, including high concentrations, and makes it possible to prepare a variety of materials via postfunctionalization or click chemistry.[50] To monitor these synthetic steps at the surface of materials with conventional room-temperature solid-state NMR would be prohibitively time-consuming (experiments typically take between 12 and 24 h for a one-dimensional carbon-13 CPMAS spectra; see the Supporting Information). In particular, acquisition of 2D correlation spectra or nitrogen-15 spectra at natural isotopic abundance is not conceivable even when they would be necessary for unambiguous assignment.

Here, DNP SENS provides a means of routine characterization, by enabling the expedient acquisition of carbon-13, nitrogen-15 and silicon-29 1D and 2D solid-state NMR spectra at natural isotopic abundances. For example, using bCTbK as a polarizing agent, high-quality 1D ^{1}H–^{13}C CPMAS spectra (10 min, Figure 4b) and a 2D ^{1}H–^{13}C correlation spectra (3.5 h, Figure 5a–d) may be acquired and allow for the complete characterization of the carbon skeletons. The nitrogen-containing functionalities were identified with ^{1}H–^{15}N CPMAS spectra (14 h each, Figure 4c). These high-quality ^{15}N CPMAS spectra even allow for minor reaction byproducts to be observed. Note that spectra with a signal-to-noise ratio of 20, high enough for routine characterization, can be acquired in 40 min (see Figure S6). A 2D ^{1}H–^{15}N correlation spectrum of **Mat-PrIm** was also acquired overnight (14 h, Figure 5e, vide infra). None of these would have been possible without the gain in sensitivity provided by DNP SENS. These results are all the more impressive considering that ^{15}N is an extremely unreceptive NMR nucleus due to its low magnetogyric ratio and low natural abundance. Note that with bTbK, experimental lengths 6 times longer would have been necessary to get the same sensitivity.

The interpretation and assignment of the DNP enhanced solid-state NMR spectra are now discussed in detail. The ^{13}C CPMAS spectra of **Mat-PrN$_3$** display three carbon resonances with chemical shifts of 8.1, 21.1, and 53.0 ppm, as expected from its proposed structure. They correlate with protons whose chemical shifts are 1.1, 2.15, and 3.2 ppm, respectively (Figure 5b), which is coherent with a propylazide moiety. The ^{15}N spectra of **Mat-PrN$_3$** display three resonances at 73.7, 219.5, and 248.5 ppm, confirming the presence of the azide group (Figure 4c). Upon conversion to **Mat-PrNH$_2$** with the

dx.doi.org/10.1021/ja210177v | J. Am. Chem.Soc. 2012, 134, 2284–2291

Staudinger reaction, the ^{13}C resonance of C_3 is shifted from 53.0 to 41.5 ppm, consistent with conversion of the azide group into an amine.

The nitrogen spectrum now displays one main resonance at 34.3 ppm, characteristic of the NH_2 group (Figure 4c). The byproducts observed on the ^{15}N spectrum at 89 ppm are attributed to a small amount of unconverted starting azide units (ca. 10%). One interpretation for the incomplete conversion is the inaccessibility of some of these organic fragments on the surface. The carbon-13 spectrum of **Mat-PrIm**, obtained subsequently upon reaction with formaldehyde, glyoxal, and benzylamine, displays resonances with chemical shifts characteristic of aromatic groups (129.2 ppm ^{13}C/6.8 ppm ^{1}H) and (122.1 ppm ^{13}C/6.8 ppm ^{1}H), as well as the three expected aliphatic resonances (Figures 4b and 5d). The ^{15}N spectrum confirms the presence of imidazolium nitrogen atoms with the most intense resonance centered at 185 ppm (the two nitrogen resonances being not resolved, Figure 4c).

The complete and detailed characterization of **Mat-PrIm** was further obtained by the acquisition of a 2D $^{1}H-^{15}N$ correlation spectrum (Figure 5e), which shows three resolved cross peaks, all consistent with the structure of **Mat-PrIm**. The cross peak at (185.6 ppm ^{15}N/8.9 ppm ^{1}H) corresponds to a correlation between the nitrogens and aromatic protons, notably the C_6-H proton. A shoulder at (131.1 ppm ^{13}C/8.9 ppm ^{1}H) can be discerned in the $^{1}H-^{13}C$ HETCOR spectra corresponding to a correlation between C_6 and this proton. The cross peak at (185.3 ppm ^{15}N/5.4 ppm ^{1}H) corresponds to the correlations between $N_{a''}$ and $N_{b''}$ and the CH_2 protons of $C_{3''}$ and C_7. The peak at (187.2 ppm ^{15}N/1.9 ppm ^{1}H) indicates the correlation between the protons of $C_{2''}$ and $N_{a''}$, which is the only nitrogen close enough for magnetization transfer with this CP contact time (1 ms). The ^{15}N chemical shift for this cross peak is slightly different from those of the previous two, confirming the presence of two distinct imidazolium nitrogens in the molecule. This analysis is confirmed by the lower intensity of this peak as compared to the other two, indicating a longer distance from the protons correlating with the other nitrogen, once again compatible with the molecular structure of **Mat-PrIm**.

The conformation of the organic moieties with respect to the surface is also important to help understand the folding of functionalities and the derived properties. A 2D $^{1}H-^{29}Si$ correlation spectrum of **Mat-PrIm** could be acquired in 10 min. The cross peak at (−64.7 ppm ^{29}Si/1.2 ppm ^{1}H) shows the expected correlations between the T site silicon atoms (silicon bonded to the carbon of the organic moiety) and the aliphatic protons of carbon $C_{1''}$ and $C_{2''}$. The cross peak at (−99.8 ppm ^{29}Si/7.6 ppm ^{1}H) shows a correlation between the Q sites silicon atoms and the aromatic protons. This correlation indicates that the imidazolium ring is in close proximity to the surface of the material and that the tether folds to maximize the interaction between the aromatic groups and the surface functionalities.[15]

In summary, the combination of the multidimensional proton, carbon, nitrogen, and silicon spectra clearly provides the mean to unambiguously and rapidly characterize these surface compounds at a molecular level. This demonstrates how, due to the large enhancements provided by the bCTbK biradical, DNP SENS can now be routinely applied to characterize materials and surface compounds.

CONCLUSION

Here, we introduced a new biradical, bCTbK, as a polarization source for DNP NMR experiments. This derivative of the well-known bTbK provides high DNP and sensitivity enhancements due to its rigid structure and absence of methyl groups, leading to slow electron relaxation and enhanced saturation of the EPR line. We expect that the very high enhancements will make this radical the polarization source of choice for the characterization of materials. As bCTbK is also a very efficient polarization source for bulk frozen solution, its applications are not limited to the study of surfaces, and it could be used for the study of proteins in lipid environments, polymers, or in dissolution DNP experiments, for instance. Design and testing of water-soluble versions of bCTbK for biological applications are currently underway.

The high efficiency of this radical was demonstrated for DNP SENS by following a series of chemical reactions on the surface of materials, monitoring the ^{13}C, ^{29}Si, ^{1}H, and ^{15}N chemical shifts at natural isotopic abundance using multidimensional correlation experiments. The reduction in experiment time by DNP SENS experiments with bCTbK is estimated to be on the order of 12 700 as compared to room-temperature experiments. These experiments would have previously been impossible to undertake at natural isotopic abundance in reasonable time. This study demonstrates that DNP SENS can be used routinely to characterize materials and surface compounds, as solution-state NMR is used today in molecular chemistry.

This work also illustrates that there is still much room for improvement of the polarization sources in DNP experiments and adds a new parameter to consider in the rational design of biradicals for DNP. Rigid radicals with bulkier functionalities are known; such radicals could have even longer electron relaxation times, which could lead to higher DNP enhancements.

ASSOCIATED CONTENT

Supporting Information

Additional experimental details of preparation of materials and radicals, measurement of quenching and enhancement factors, comparison of radical efficiency, and ^{15}N NMR spectra of **Mat-PrN$_3$**, **Mat-PrNH$_2$**, and **Mat-PrIm**. This material is available free of charge via the Internet at http://pubs.acs.org.

AUTHOR INFORMATION

Corresponding Author

paul.tordo@univ-provence.fr; lyndon.emsley@ens-lyon.fr

ACKNOWLEDGMENTS

A.J.R. acknowledges support from a EU Marie-Curie IIF Fellowship (PIIF-GA-2010-274574). Financial support is acknowledged from EQUIPEX contract ANR-10-EQPX-47-01, and the ETH Zürich. We acknowledge A. Roussey for the preparation of **Mat-PhOH**.[36]

REFERENCES

(1) Overhauser, A. *Phys. Rev.* **1953**, *92*, 411−415.
(2) Carver, T.; Slichter, C. P. *Phys. Rev.* **1953**, *92*, 212−213.
(3) Carver, T. *Phys. Rev.* **1956**, *102*, 975−981.
(4) Becerra, L.; Gerfen, G.; Temkin, R.; Singel, D.; Griffin, R. *Phys. Rev. Lett.* **1993**, *71*, 3561−3564.
(5) Rosay, M.; Tometich, L.; Pawsey, S.; Bader, R.; Schauwecker, R.; Blank, M.; Borchard, P. M.; Cauffman, S. R.; Felch, K. L.; Weber, R.

T.; Temkin, R. J.; Griffin, R. G.; Maas, W. E. *Phys. Chem. Chem. Phys.* **2010**, *12*, 5850−5860.
(6) Hall, D. A.; Maus, D. C.; Gerfen, G. J.; Inati, S. J.; Becerra, L. R.; Dahlquist, F. W.; Griffin, R. G. *Science* **1997**, *276*, 930−932.
(7) Rosay, M.; Zeri, A.-C.; Astrof, N. S.; Opella, S. J.; Herzfeld, J.; Griffin, R. G. *J. Am. Chem. Soc.* **2001**, *123*, 1010−1011.
(8) Bajaj, V. S.; Mak Jurkauskas, M. L.; Belenky, M.; Herzfeld, J.; Griffin, R. G. *Proc. Natl. Acad. Sci. U.S.A.* **2009**, *106*, 9244−9249.
(9) Salnikov, E.; Rosay, M.; Pawsey, S.; Ouari, O.; Tordo, P.; Bechinger, B. *J. Am. Chem. Soc.* **2010**, *132*, 5940−5941.
(10) Akbey, Ü.; Franks, W. T.; Linden, A.; Lange, S.; Griffin, R. G.; van Rossum, B.-J.; Oschkinat, H. *Angew. Chem., Int. Ed.* **2010**, *49*, 7803−7806.
(11) van der Wel, P. C. A.; Hu, K.-N.; Lewandowski, J.; Griffin, R. G. *J. Am. Chem. Soc.* **2006**, *128*, 10840−10846.
(12) Debelouchina, G. T.; Bayro, M. J.; van der Wel, P. C. A.; Caporini, M. A.; Barnes, A. B.; Rosay, M.; Maas, W. E.; Griffin, R. G. *Phys. Chem. Chem. Phys.* **2010**, *12*, 5911−5919.
(13) Bayro, M. J.; Debelouchina, G. T.; Eddy, M. T.; Birkett, N. R.; MacPhee, C. E.; Rosay, M.; Maas, W. E.; Dobson, C. M.; Griffin, R. G. *J. Am. Chem. Soc.* **2011**, *133*, 13967−13974.
(14) Lesage, A.; Lelli, M.; Gajan, D.; Caporini, M. A.; Vitzthum, V.; Miéville, P.; Alauzun, J.; Roussey, A.; Thieuleux, C.; Mehdi, A.; Bodenhausen, G.; Copéret, C.; Emsley, L. *J. Am. Chem. Soc.* **2010**, *132*, 15459−15461.
(15) Lelli, M.; Gajan, D.; Lesage, A.; Caporini, M. A.; Vitzthum, V.; Miéville, P.; Héroguel, F.; Rascón, F.; Roussey, A.; Thieuleux, C.; Boualleg, M.; Veyre, L.; Bodenhausen, G.; Copéret, C.; Emsley, L. *J. Am. Chem. Soc.* **2011**, *133*, 2104−2107.
(16) Lafon, O.; Rosay, M.; Aussenac, F.; Lu, X.; Trébosc, J.; Cristini, O.; Kinowski, C.; Touati, N.; Vezin, H.; Amoureux, J.-P. *Angew. Chem., Int. Ed.* **2011**, *50*, 8367−8370.
(17) Rossini, A. J.; Zagdoun, A.; Lelli, M.; Gajan, D.; Rascon, F.; Rosay, M.; Maas, W. E.; Coperet, C.; Emsley, L.; Lesage, A. *Chem. Sci.* **2012**, *3*, 108−115.
(18) Maly, T.; Debelouchina, G. T.; Bajaj, V. S.; Hu, K.-N.; Joo, C.-G.; Mak Jurkauskas, M. L.; Sirigiri, J. R.; van der Wel, P. C. A.; Herzfeld, J.; Temkin, R. J.; Griffin, R. G. *J. Chem. Phys.* **2008**, *128*, 052211.
(19) Hu, K.-N.; Yu, H.-H.; Swager, T. M.; Griffin, R. G. *J. Am. Chem. Soc.* **2004**, *126*, 10844−10845.
(20) Hu, K.-N.; Debelouchina, G. T.; Smith, A. A.; Griffin, R. G. *J. Chem. Phys.* **2011**, *134*, 125105.
(21) Hu, K.-N. *Solid State Nucl. Magn. Reson.* **2011**, *40*, 31−41.
(22) Song, C.; Hu, K.-N.; Joo, C.-G.; Swager, T. M.; Griffin, R. G. *J. Am. Chem. Soc.* **2006**, *128*, 11385−11390.
(23) Thurber, K. R.; Yau, W.-M.; Tycko, R. *J. Magn. Reson.* **2010**, *204*, 303−313.
(24) Ysacco, C.; Rizzato, E.; Virolleaud, M.-A.; Karoui, H.; Rockenbauer, A.; Le Moigne, F.; Siri, D.; Ouari, O.; Griffin, R. G.; Tordo, P. *Phys. Chem. Chem. Phys.* **2010**, *12*, 5841−5845.
(25) Hu, K.-N.; Song, C.; Yu, H.-H.; Swager, T. M.; Griffin, R. G. *J. Chem. Phys.* **2008**, *128*, 052302.
(26) Matsuki, Y.; Maly, T.; Ouari, O.; Karoui, H.; Le Moigne, F.; Rizzato, E.; Lyubenova, S.; Herzfeld, J.; Prisner, T.; Tordo, P.; Griffin, R. G. *Angew. Chem., Int. Ed.* **2009**, *48*, 4996−5000.
(27) Hu, K.-N.; Bajaj, V. S.; Rosay, M.; Griffin, R. G. *J. Chem. Phys.* **2007**, *126*, 044512.
(28) Dane, E. L.; Maly, T.; Debelouchina, G. T.; Griffin, R. G.; Swager, T. M. *Org. Lett.* **2009**, *11*, 1871−1874.
(29) Corzilius, B.; Smith, A. A.; Barnes, A. B.; Luchinat, C.; Bertini, I.; Griffin, R. G. *J. Am. Chem. Soc.* **2011**, *133*, 5648−5651.
(30) Barnes, A. B.; De Paëpe, G.; van der Wel, P. C. A.; Hu, K. N.; Joo, C. G.; Bajaj, V. S.; Mak-Jurkauskas, M. L.; Sirigiri, J. R.; Herzfeld, J.; Temkin, R. J.; Griffin, R. G. *Appl. Magn. Reson.* **2008**, *34*, 237−263.
(31) Zagdoun, A.; Rossini, A. J.; Gajan, D.; Bourdolle, A.; Ouari, O.; Rosay, M.; Maas, W. E.; Tordo, P.; Lelli, M.; Emsley, L.; Lesage, A.; Coperet, C. *Chem. Commun.* **2012**, *48*, 654−656.
(32) Casabianca, L. B.; Shames, A. I.; Panich, A. M.; Shenderova, O.; Frydman, L. *J. Phys. Chem. C* **2011**, *115*, 19041−19048.
(33) Matsuki, Y.; Takahashi, H.; Ueda, K.; Idehara, T.; Ogawa, I.; Toda, M.; Akutsu, H.; Fujiwara, T. *Phys. Chem. Chem. Phys.* **2010**, *12*, 5799−5803.
(34) Sato, H.; Kathirvelu, V.; Fielding, A.; Blinco, J. P.; Micallef, A. S.; Bottle, S. E.; Eaton, S. S.; Eaton, G. R. *Mol. Phys.* **2007**, *105*, 2137−2151.
(35) Kathirvelu, V.; Smith, C.; Parks, C.; Mannan, M. A.; Miura, Y.; Takeshita, K.; Eaton, S. S.; Eaton, G. R. *Chem. Commun.* **2009**, 454−456.
(36) Roussey, A.; Gajan, D.; Maishal, T. K.; Mukerjee, A.; Veyre, L.; Lesage, A.; Emsley, L.; Copéret, C.; Thieuleux, C. *Phys. Chem. Chem. Phys.* **2011**, *13*, 4230−4233.
(37) Sakai, K.; Yamada, K.-I.; Yamasaki, T.; Kinoshita, Y.; Mito, F.; Utsumi, H. *Tetrahedron* **2010**, *66*, 2311−2315.
(38) Fung, B. M.; Khitrin, A. K.; Ermolaev, K. *J. Magn. Reson.* **2000**, *142*, 97−101.
(39) Blanc, F.; Copéret, C.; Lesage, A.; Emsley, L. *Chem. Soc. Rev.* **2008**, *37*, 518−526.
(40) Vitzthum, V.; Mieville, P.; Carnevale, D.; Caporini, M. A.; Gajan, D.; Coperet, C.; lelli, M.; Zagdoun, A.; Rossini, A. J.; Lesage, A.; Emsley, L.; Bodenhausen, G. *Chem. Commun.*, submitted.
(41) Rossini, A. J.; Zagdoun, A.; Lelli, M.; Canivet, J.; Aguado, S.; Ouari, O.; Tordo, P.; Rosay, M.; Maas, W. E.; Coperet, C.; Farrusseng, D.; Emsley, L.; Lesage, A. *Angew. Chem., Int. Ed.*, in press, DOI: 10.1002/anie.201106030.
(42) Kang, T.; Oh, S.; Kim, H.; Yi, J. *Langmuir* **2005**, *21*, 5859−5864.
(43) Sasaki, T.; Zhong, C.; Tada, M.; Iwasawa, Y. *Chem. Commun.* **2005**, 2506−2508.
(44) Lungwitz, R.; Linder, T.; Sundermeyer, J.; Tkatchenko, I.; Spange, S. *Chem. Commun.* **2010**, *46*, 5903−5905.
(45) Vangeli, O. C.; Romanos, G. E.; Beltsios, K. G.; Fokas, D.; Kouvelos, E. P.; Stefanopoulos, K. L.; Kanellopoulos, N. K. *J. Phys. Chem. B* **2010**, *114*, 6480−6491.
(46) Nguyen, T. P.; Hesemann, P.; Moreau, J. J. E. *Microporous Mesoporous Mater.* **2011**, *142*, 292.
(47) Maishal, T. K.; Alauzun, J.; Basset, J.-M.; Copéret, C.; Corriu, R. J. P.; Jeanneau, E.; Mehdi, A.; Reyé, C.; Veyre, L.; Thieuleux, C. *Angew. Chem., Int. Ed.* **2008**, *47*, 8654−8656.
(48) Karamé, I.; Boualleg, M.; Camus, J.-M.; Maishal, T. K.; Alauzun, J.; Basset, J.-M.; Copéret, C.; Corriu, R. J. P.; Jeanneau, E.; Mehdi, A.; Reyé, C.; Veyre, L.; Thieuleux, C. *Chem.-Eur. J.* **2009**, *15*, 11820−11823.
(49) Hoffmann, F.; Cornelius, M.; Morell, J.; Fröba, M. *Angew. Chem., Int. Ed.* **2006**, *45*, 3216−3251.
(50) Nakazawa, J.; Stack, T. D. P. *J. Am. Chem. Soc.* **2008**, *130*, 14360−14361.
(51) Elena, B.; De Paëpe, G.; Emsley, L. *Chem. Phys. Lett.* **2004**, *398*, 532−538.